Published in final edited form as:
Cell Rep. 2013 June 27; 3(6): 1840–1846. doi:10.1016/j.celrep.2013.05.025.

The transcription factor IRF3 triggers "defensive suicide" necrosis in response to viral and bacterial pathogens

Nelson C. Di Paolo[1], **Konstantin Doronin**[1,3], **Lisa K. Baldwin**[1], **Thalia Papayannopoulou**[2], and **Dmitry M. Shayakhmetov**[1,*]

[1]Division of Medical Genetics, Department of Medicine, University of Washington, Seattle, WA, 98195, USA

[2]Division of Hematology, Department of Medicine, University of Washington, Seattle, WA, 98195, USA

SUMMARY

Although molecular components that execute non-inflammatory apoptotic cell death are well defined, molecular pathways that trigger necrotic cell death remain poorly characterized. Here we show that in response to infection with adenovirus or *Listeria monocytogenes*, macrophages *in vivo* undergo rapid pro-inflammatory necrotic death that is controlled by interferon-regulatory factor 3 (IRF3). The transcriptional activity of IRF3 is, surprisingly, not required for the induction of necrosis, and it proceeds normally in mice deficient in all known regulators of necrotic death or IRF3 activation, including RIPK3, Caspases-1, -8, or -11, STING and IPS1/MAVS. Although *L.monocytogenes* triggers necrosis to promote the infection, IRF3-dependent necrosis is required for reducing pathogen burden in the models of disseminated infection with adenovirus. Therefore, our studies implicate IRF3 as a principal and non-redundant component of a novel physiologically-regulated necrotic cell death pathway that operates as an effective innate immune mechanism of host protection against disseminated virus infection.

INTRODUCTION

Physiologically regulated cell death is a fundamental process in multi-cellular organisms that is critical for host survival. Although molecular components that execute non-inflammatory apoptotic cell death are well defined, molecular pathways that trigger regulated pro-inflammatory necrotic cell death remain poorly characterized. In response to pathogens, damage, or stress, cells can undergo capsase-1-dependent pro-inflammatory type of cell death called pyroptosis (Bergsbaken et al., 2009). Under the conditions when apoptotic caspases are blocked, in response to pleiotropic cytokine TNF-α or Fas-ligand, cells can undergo RIPK1-RIPK3-dependent necroptosis (Kaczmarek et al., 2013). Cells dieing via caspase-1-dependent pyroptosis and RIPK1-RIPK3-dependent necroptosis exhibit

*Correspondence: dshax@uw.edu.
[3]current address: Department of Molecular Microbiology and Immunology St. Louis University, St. Louis, MO, 63104, USA

SUPPLEMENTAL INFORMATION

Supplemental Information includes Extended Experimental Procedures, three figures, one table, and supplemental references and can be found with this article online at http://

similar morphological changes that include lack of chromatin condensation and the loss of plasma membrane integrity.

Human adenovirus (HAdv) is a common human pathogen and for immunocompromized individuals, HAdv infections can be lethal (Kojaoghlanian et al., 2003). Accumulated data with using wild type HAdv species and HAdv-based vectors in pre-clinical studies and clinical gene therapy trials demonstrate that virus particles are efficiently cleared from the blood by resident liver macrophages Kupffer cells (Lieber et al., 1997; Morral et al., 2002). However, after interaction with the virus, Kupffer cells undergo rapid death (Manickan et al., 2006) and molecular pathways triggering this response and its physiological relevance remain undefined.

Here we show that IRF3 is a principal and non-redundant factor that triggers rapid necrotic macrophage cell death *in vivo* in response to disseminated infections with adenovirus or *L.monocytogenes*. The activation of this IRF3-dependent cell death is associated with the loss of plasma membrane integrity within minutes after the pathogen challenge and, remarkably, does not require IRF3-dependent gene expression. Although *L.monocytogenes* triggers IRF3-dependent necrosis to promote the infection, macrophage necrosis is required for reducing pathogen burden in the models of disseminated infection with adenovirus. Collectively, our studies reveal a novel physiologically-regulated necrotic cell death pathway that operates as an effective innate immune mechanism of host protection against disseminated virus infection.

RESULTS

HAdv triggers necrotic type of macrophage death *in vivo*, independently of caspase-1, caspase-8, caspase-11, and RIPK3

To classify the type of death that Kupffer cells undergo after exposure to HAdv (Galluzzi et al., 2012), we utilized an all *in vivo* approach and challenged mice deficient in principal mediators of the known specific regulated cell death mechanisms and immune pathways with the virus (Table S1). Intravenous injection of wild type HAdv into wild type mice resulted in efficient trapping of virus particles by $CD68^+$ resident liver macrophages (Figure 1A). Furthermore, subsequent administration of mice with membrane impermeable dye propidium iodide (PI) revealed that nuclei of all $CD68^+$ cells were stained PI-positive, demonstrating that these cells have lost their plasma membrane integrity (Figures 1B and S1A). Mice deficient in inflammatory and apoptotic caspases demonstrated no reduction in sensitivity of liver macrophages to HAdv challenge (Figure 1C). HAdv administration to mice deficient in various inflammatory cytokines, toll-like receptors, cathepsins -B, -L, and -S, superoxide producing NADPH oxidase components $p47^{Phox}$ and $gp91^{Phox}$, pro-apoptotic proteins BAK and BAX, or mitochondrial Cyclophillin D (*Ppif*$^{-/-}$) showed lack of resistance of liver macrophages to the virus (Figures S1C-F). Furthermore, HAdv administration to mice deficient in key mediators of pyronecrosis (ASC-deficient *Pycard*$^{-/-}$), necroptosis (*Ripk3*$^{-/-}$ and *Casp8*$^{-/-}$/*Ripk3*$^{-/-}$), stress response PIDDosome (RAIDD-deficient mice, *Cradd*$^{-/-}$), *Myd88*$^{-/-}$, and *Ticam1*$^{-/-}$ demonstrated their sensitivity to the virus (Figure 1D). The analysis of the kinetics of plasma membrane integrity loss revealed that within 10 minutes after the virus administration, nuclei of all liver macrophages became PI-positive (Figure 1E). Ultrastructural analysis of liver macrophages 15 minutes after the virus challenge revealed catastrophic disorganization of the cytosol and swollen mitochondria (Figures 1F). Administration of HAdv into mice also resulted in significant increase in the amount of cytosolic enzyme lactate dehydrogenase (LDH) in plasma, compared to saline-injected group (Fig. 1G). Collectively, the ultrastructural changes, along with the loss of the plasma membrane integrity, are consistent with morphological and functional changes associated with necrotic forms of cell death (Ting et al., 2008). However, this necrotic-type

cell death occurs with extremely rapid kinetics and independently of the known principal mediators that execute both apoptotic and necrotic cell death programs (Galluzzi et al., 2012).

Macrophages in *Irf3*$^{-/-}$ are resistant to virus-induced necrotic cell death

Next we extended our analyses to mice deficient in mediators of virus infection-sensing pathways. This analysis revealed that in mice deficient in transcriptional factor interferon regulatory factor 3 (IRF3) (Sato et al., 2000), liver macrophages were resistant to HAdv-induced cell death (Figures 2A-C, and S2). Furthermore, in *Irf3*$^{-/-}$ mice, CD68^{+} cells were present in the liver parenchyma even 24 hours after the virus challenge (Figures 2B-C). Surprisingly, CD68^{+} cells in the livers of mice deficient in IPS-1/MAVS/VISA (Kawai et al., 2005; Meylan et al., 2005; Seth et al., 2005; Xu et al., 2005) and STING (Ishikawa and Barber, 2008; Sauer et al., 2011b), that operate upstream of IRF3 in viral genome-sensing pathways, as well as in mice deficient in cytosolic DNA sensor DAI (*Zbp1*$^{-/-}$) (Takaoka et al., 2007) were sensitive to HAdv challenge (Figures 2A-B).

Because activation of IRF3 as a transcription activation factor associates with its phosphorylation at Ser396 (Yoneyama et al., 2002), we analyzed whether IRF3 is phosphorylated at Ser396 by the time of macrophage cell death. Western blot analysis showed that IRF3 became phosphorylated at Ser396 in response to cell treatment with poly-I:C *in vitro*, however, Ser396 IRF3 phosphorylation was lacking in both saline and HAdv-treated mice (Figures 2D-E). The analysis of IRF3-dependent gene expression in the liver and spleen (Figures 2F-G) by 30 minutes after the virus challenge further revealed the lack of transcriptional activation of IRF3-dependent genes.

Necrotic-type cell death associates with systemic inflammatory response syndrome that can be lethal to the host (Kaczmarek et al., 2013). Therefore, we challenged *WT* and *Irf3*$^{-/-}$ mice with HAdv and analyzed plasma cytokines and chemokines 1 hour after virus administration. This analysis showed that numerous pro-inflammatory cytokines and chemokines, including IL-1α, IL-16, GM-CSF, CCL1, CCL4, CCL11, CXCL1 and CXCL2, were elevated in plasma of *WT*, but not *Irf3*$^{-/-}$ mice after the virus challenge (Figure 2H-I). Consistent with the reduced levels of cytokines and chemokines, cytopenia (a clinical marker of systemic inflammatory response), was not observed in *Irf3*$^{-/-}$ mice after the virus challenge, while *WT* mice were highly cytopenic after the virus infection (Figure 2J).

IRF3 triggers macrophage necrosis upon pathogen entry into the cytosol

Earlier analyses suggested that HAdv entry into the cytosol is required for the induction of macrophage cell death *in vivo* (Smith et al., 2008). However, many viral and bacterial pathogens target cytosol as an effective reproductive niche within the cell. Therefore, we infected mice with wild type adenovirus serotypes HAdv2, HAdv5, replication-defective adenovirus vector Ad5GFP, or a single-point HAdv2 mutant *ts1*, that cannot escape from the endosomal compartment into the cytosol (Greber et al., 1993). We also infected mice with wild type *Listeria monocytogenes* as a representative facultative cytosolic bacterial pathogen or its isogenic mutant Δ*hly* that lacks Listeriolysin O and fails to escape from the phagosomal compartment into the cytosol (Portnoy et al., 1988). The analysis of the loss of plasma membrane integrity by liver macrophages after *WT* mice infection with all of these pathogens showed that liver macrophages rapidly became PI-permeable in response to HAdv2, HAdv5, Ad5GFP vector, and *L.monocytogenes* infection (Figure 3A). However, both the *ts1* adenovirus and Δ*hly L.monocytogenes* mutant failed to induce permeability of liver macrophages to PI (Figures 3A and S3). Remarkably, macrophages in *Irf3*$^{-/-}$ mice did not lose plasma membrane integrity after infection with all of these pathogens (Figures 3A-C and S3). We further confirmed that CD68^{+} liver macrophages efficiently sequester

L.monocytogenes from the blood (Figure 3B), and liver macrophage permeability to the PI after *L.monocytogenes* infection associates with elevated LDH levels in plasma in *WT* but not *Irf3*$^{-/-}$ mice, demonstrating that upon entry into macrophages *in vivo*, *L.monocytogenes* triggers genuine and rapid physiologically-regulated necrosis, that requires pathogen entry into the cytosol. Similar to results observed with mouse infection with HAdv, we found that liver macrophages became PI-permeable after *L.monocytogenes* infection of mice deficient in inflammasome components ASC, Caspase-1 and -11, Cathepsin-B, STING, and IPS1/MAVS, but not in *Irf3*$^{-/-}$ mice (Fig. 3E). Collectively, these data demonstrate that IRF3 triggers necrosis *in vivo* in response to both HAdv and *L.monocytogenes* infection. Furthermore, pathogen penetration into the cytosol is required to induce this form of necrosis.

IRF3-dependent "defensive suicide" is a protective macrophage effector mechanism against disseminated virus infection

To analyze functional relevance of IRF3-dependent macrophage necrosis for host defense against disseminated infections, we first infected *WT* and *Irf3*$^{-/-}$ mice with *L.monocytogenes* and analyzed pathogen burden in the liver 6 h post infection. This analysis showed that the bacterial burden doubled over this timeframe, but only in *WT* and not in *Irf3*$^{-/-}$ mice (Figure 4A). In contrast, upon infection of *WT* and *Irf3*$^{-/-}$ mice with wild type HAdv5, 24 h post infection, the pathogen burden was significantly higher in the livers of mice deficient in IRF3, compared to control *WT* mice (Figure 4B).

The observation that macrophages induce IRF3-dependent necrotic death within minutes after interaction with HAdv may indicate that this form of regulated necrosis functionally represents a "defensive suicide" strategy that must be effective at enabling immunity to disseminated virus infection. Consequently, for the host that lacks this macrophage population, even a sub-lethal virus infection may lead to compromised resistance and be detrimental to survival. To experimentally evaluate this assumption, we depleted wild type mice of tissue macrophages with clodronate liposomes prior to their challenge with escalating sub-lethal doses of the wild type HAdv5 and compared the virus burden in the liver 48 hours after virus administration. This analysis revealed that in mice depleted of tissue macrophages, there was 2 to 3 orders of magnitude higher virus DNA burden compared to mice with liver macrophages intact (Figure 4C). The serum levels of liver enzymes ALT and AST, indicating virus-induced hepatotoxicity, were significantly (up to 10-fold) higher in macrophage-depleted mice, compared to mice with tissue macrophages (Figure 4D). Furthermore, depletion of tissue macrophages from mice resulted in over 10-fold reduction in LD_{50}, extensive histologically-evident liver damage, virus replication and protein expression (Figs. 4E-G). At a sub-lethal doses of 10^{10} and 10^{11} virus particles per mouse, the majority of macrophage-containing mice survived the infection for the duration of the experiment (250 hours post virus infection), while 100% of macrophage-depleted mice succumbed by 75 hours ($P<0.0006$) (Fig. 4H). Collectively, these data provide experimental evidence that HAdv-triggered macrophage cell death effectively reduces the virus burden and protects the host from sub-lethal doses of disseminated virus *in vivo*.

DISCUSSION

In this study we implicated IRF3 as a critical and non-redundant factor required for the execution of novel necrotic cell death type that ensues in response to viral and bacterial pathogens. We found that upon triggering necrotic death, IRF3 does not function as a transcription activating factor. Although IRF3 can be activated downstream of the IPS1/MAVS/VISA- and STING-mediated viral genome sensing pathway as well as TBK1/IKKε signaling in various cell types (Fitzgerald et al., 2003; Takeuchi and Akira, 2009), our data indicate that in the context of IRF3-dependent necrosis, both IPS1/MAVS and STING, as

well as BAK and BAX (Chattopadhyay et al., 2010; Chattopadhyay et al., 2011) are all dispensable for the induction and execution of cell death *in vivo*. Using the entirely genetic evidence in mice deficient in Cathepsin B, inflammasome component ASC (that is required for NLRP3-mediated inflammasome activation), Caspases-1 and -11, as well as ROS-producing NADPH-oxidase components $p47^{Phox}$ and $gp91^{Phox}$, we found that liver macrophages rapidly lose their plasma membrane integrity after HAdv infection indicating that IRF3-dependent necrosis is a distinct pathway and requires none of these components to ensue *in vivo*.

Caspase-1-dependent pyroptosis is an important host defense mechanism and constitutes a necrotic-type cell death that ablates the niche for pathogen replication (Bergsbaken et al., 2009). However, pyroptosis *per se* does not result in the reduction of pathogen burden and, to control the infection, bacteria released from pyroptotic cells *in vivo* are killed by bactericidal effectors produced by host's neutrophils (Miao et al., 2010). Here we showed that the induction of IRF3-dependent necrosis *in vivo* does not result in the reduction of *L.monocytogenes* burden in the liver but, rather, it supports the infection. It is noteworthy that *L.monocytogenes* that was engineered to ectopically expresses *Legionella pneumophila* flagellin and, therefore, became highly efficient at activating NLRC4 inflammasome, *in vivo* exhibited a severely attenuated phenotype, compared to parental *L.monocytogenes* strain (Sauer et al., 2011a). Together this data suggests that bacterial pathogens may have evolved specific mechanisms to activate pro-inflammatory nectoric-type cell death *in vivo* to propagate the infection, likely via the recruitment of pathogen-susceptible monocytes. However, a delicate balance may exist where an excessive or untimely pro-inflammatory cell death limits pathogen survival.

The unique feature of the IRF3-dependent necrosis is its extremely rapid kinetic that enables host protection from disseminated virus infection. RIPK1-RIPK3-dependent necroptosis was shown to play a key role in development and immunity (Declercq et al., 2009; Green et al., 2011). However, in response to physiological stimuli, necroptosis occurs with much slower kinetics and was shown to be targeted by specific viral genes to prevent cell death execution (Upton et al., 2010; Upton et al., 2012). Our finding of IRF3-dependent cell death may also be relevant to conditions and pathologies beyond host responses to disseminated infections with viral and bacterial pathogens. The development of specific pharmacological inhibitors of this novel regulated necrotic cell death type may reveal its contribution and be found useful for the treatment of inflammatory diseases and conditions where underlying pathology is associated with perpetual cycles of pro-inflammatory cell death.

EXPERIMENTAL PROCEDURES

All animal studies were carried out with the approval of the Institutional Animal Care and Use Committee of the University of Washington, Seattle, WA. C57BL/6 mice were purchased from Charles River, Wilmington, MA. All mice were on C57BL/6 genetic background, matched by age and housed in specific-pathogen-free facilities. Mice were infected with wild type HAdv at a dose of 1×10^{10} virus particles per mouse via tail vein infusion. Viral particle titers were determined by OD_{260} measurement. For *in vivo* experiments, only virus preparations confirmed to be free of endotoxin contamination were used. *L.monocytogenes* and isogenic Δ*hly* strains were grown on BHI plates from frozen stocks. Stationary cultures were initiated from single colonies and incubated at 30C overnight. Two to 4 hours prior to bacteria administration into mice at a dose of 10^8 CFU via the tail vein infusion, fresh cultures were initiated and incubated at 37C with shaking as described in (Sauer et al., 2011a). Bacteria titers were measured by optical density and verified by plating serial 10-fold dilutions on BHI plates. Administration of this dose of *L.monocytogenes* into the bloodstream resulted in deposition of 1-2 visible bacterial cells

per liver macrophage (determined by injecting CFSC-labeled bacteria). Proteome Profiler antibody array "Mouse Cytokine Array Panel A" (#ARY006) was from R&D Systems and was used according to the manufacturer's instructions. Unless otherwise noted, statistical analysis in each independent experiment was performed with an unpaired, two-tailed Student's *t*-test. Data are reported as mean ± standard deviation. $P < 0.05$ was considered statistically significant. Animal survival was analyzed using log-rank test and GraphPad Prism 5 software.

Supplementary Material

Refer to Web version on PubMed Central for supplementary material.

Acknowledgments

We thank Drs. V. Dixit (Roche, CA) for *Pycard*$^{-/-}$ and *Ripk3*$^{-/-}$, R.A. Flavell (Yale University, CT) for *Casp1/1*$^{-/-}$, S. Akira (Osaka University, Japan) for *Myd88*$^{-/-}$, *Tlr4*$^{-/-}$, *Tlr7/8*$^{-/-}$, *Tlr9*$^{-/-}$, and *Zbp1*$^{-/-}$, R.Vance (University of California, Berkeley, CA) for *Tmem173*$^{Gt/Gt}$, M. Gale Jr. (University of Washington, WA) for *Sti*$^{-/-}$ (*Mavs*$^{-/-}$), R. Hakem (University of Toronto, ON, Canada) for *Casp8*$^{fl/fl}$, S. Hedrick (University of California, San Diego, CA) for *Casp8*$^{fl/fl}$, D. Green (St. Jude Children's Research Hospital, Memphis, TN) for *Casp8*$^{-/-}$*Ripk3*$^{-/-}$, T. Mak (University Health Network, ON, Canada) for *Cradd*$^{-/-}$, T. Reinheckel (Albert-Ludwigs-University Freiburg, Freiburg, Germany) and J. Joyce (Memorial Sloan-Kettering Cancer Center, NY) for *Ctsb*$^{-/-}$, *Ctss*$^{-/-}$ and *Ctsl*$^{-/-}$, Y. Iwakura (University of Tokyo, Japan) for *Il1a*$^{-/-}$ and *Il1a/b*$^{-/-}$, D. Chaplin (University of Alabama, AL) for *Il1b*$^{-/-}$, M. Wewers (Ohio State University, OH) for *Il1b*$^{-/-}$/*Il18*$^{-/-}$, and T. Taniguchi (University of Tokyo) for *Irf3*$^{-/-}$ mice . We are thankful to A. Byrnes (US Food and Drug Administration) for providing *ts1* virus. *L.monocytogenes* (10403S) and isogenic Δ*hly* strains were provided by E. Miao (University of North Carolina, Chapel Hill, USA) and A. Aderem (SeattleBiomed, USA). This study was supported by US NIH grants AI065429 and CA141439 to D.M.S.

REFERENCES

Bergsbaken T, Fink SL, Cookson BT. Pyroptosis: host cell death and inflammation. Nature Reviews Microbiology. 2009; 7:99–109.

Chattopadhyay S, Marques JT, Yamashita M, Peters KL, Smith K, Desai A, Williams BRG, Sen GC. Viral apoptosis is induced by IRF-3-mediated activation of Bax. Embo Journal. 2010; 29:1762–1773. [PubMed: 20360684]

Chattopadhyay S, Yamashita M, Zhang Y, Sen GC. The IRF-3/Bax-Mediated Apoptotic Pathway, Activated by Viral Cytoplasmic RNA and DNA, Inhibits Virus Replication. Journal of Virology. 2011; 85:3708–3716. [PubMed: 21307205]

Declercq W, Vanden Berghe T, Vandenabeele P. RIP Kinases at the Crossroads of Cell Death and Survival. Cell. 2009; 138:229–232. [PubMed: 19632174]

Fitzgerald KA, McWhirter SM, Faia KL, Rowe DC, Latz E, Golenbock DT, Coyle AJ, Liao SM, Maniatis T. IKKepsilon and TBK1 are essential components of the IRF3 signaling pathway. Nat Immunol. 2003; 4:491–496. [PubMed: 12692549]

Galluzzi L, Vitale I, Abrams JM, Alnemri ES, Baehrecke EH, Blagosklonny MV, Dawson TM, Dawson VL, El-Deiry WS, Fulda S, et al. Molecular definitions of cell death subroutines: recommendations of the Nomenclature Committee on Cell Death 2012. Cell Death and Differentiation. 2012; 19:107–120. [PubMed: 21760595]

Greber UF, Willetts M, Webster P, Helenius A. Stepwise dismantling of adenovirus 2 during entry into cells. Cell. 1993; 75:477–486. [PubMed: 8221887]

Green DR, Oberst A, Dillon CP, Weinlich R, Salvesen GS. RIPK-Dependent Necrosis and Its Regulation by Caspases: A Mystery in Five Acts. Molecular Cell. 2011; 44:9–16. [PubMed: 21981915]

Ishikawa H, Barber GN. STING is an endoplasmic reticulum adaptor that facilitates innate immune signalling (vol 455, pg 674, 2008). Nature. 2008; 456:274–274.

Kaczmarek A, Vandenabeele P, Krysko DV. Necroptosis: the release of damage-associated molecular patterns and its physiological relevance. Immunity. 2013; 38:209–223. [PubMed: 23438821]

Kawai T, Takahashi K, Sato S, Coban C, Kumar H, Kato H, Ishii KJ, Takeuchi O, Akira S. IPS-1, an adaptor triggering RIG-I- and Mda5-mediated type I interferon induction. Nature Immunology. 2005; 6:981–988. [PubMed: 16127453]

Kojaoghlanian T, Flomenberg P, Horwitz MS. The impact of adenovirus infection on the immunocompromised host. Rev Med Virol. 2003; 13:155–171. [PubMed: 12740831]

Lieber A, He CY, Meuse L, Schowalter D, Kirillova I, Winther B, Kay MA. The role of Kupffer cell activation and viral gene expression in early liver toxicity after infusion of recombinant adenovirus vectors. J Virol. 1997; 71:8798–8807. [PubMed: 9343240]

Manickan E, Smith JS, Tian J, Eggerman TL, Lozier JN, Muller J, Byrnes AP. Rapid Kupffer cell death after intravenous injection of adenovirus vectors. Molecular Therapy. 2006; 13:108–117. [PubMed: 16198149]

Meylan E, Curran J, Hofmann K, Moradpour D, Binder M, Bartenschlager R, Tschopp R. Cardif is an adaptor protein in the RIG-I antiviral pathway and is targeted by hepatitis C virus. Nature. 2005; 437:1167–1172. [PubMed: 16177806]

Miao EA, Leaf IA, Treuting PM, Mao DP, Dors M, Sarkar A, Warren SE, Wewers MD, Aderem A. Caspase-1-induced pyroptosis is an innate immune effector mechanism against intracellular bacteria. Nature Immunology. 2010; 11:1136–U1194. [PubMed: 21057511]

Morral N, O'Neal WK, Rice K, Leland MM, Piedra PA, Aguilar-Cordova E, Carey KD, Beaudet AL, Langston C. Lethal toxicity, severe endothelial injury, and a threshold effect with high doses of an adenoviral vector in baboons. Hum Gene Ther. 2002; 13:143–154. [PubMed: 11779418]

Portnoy DA, Jacks PS, Hinrichs DJ. Role of hemolysin for the intracellular growth of Listeria monocytogenes. J Exp Med. 1988; 167:1459–1471. [PubMed: 2833557]

Sato M, Suemori H, Hata N, Asagiri M, Ogasawara K, Nakao K, Nakaya T, Katsuki M, Noguchi S, Tanaka N, Taniguchi T. Distinct and essential roles of transcription factors IRF-3 and IRF-7 in response to viruses for IFN-alpha/beta gene induction. Immunity. 2000; 13:539–548. [PubMed: 11070172]

Sauer JD, Pereyre S, Archer KA, Burke TP, Hanson B, Lauer P, Portnoy DA. Listeria monocytogenes engineered to activate the Nlrc4 inflammasome are severely attenuated and are poor inducers of protective immunity. Proc Natl Acad Sci U S A. 2011a; 108:12419–12424. [PubMed: 21746921]

Sauer JD, Sotelo-Troha K, von Moltke J, Monroe KM, Rae CS, Brubaker SW, Hyodo M, Hayakawa Y, Woodward JJ, Portnoy DA, Vance RE. The N-Ethyl-N-Nitrosourea-Induced Goldenticket Mouse Mutant Reveals an Essential Function of Sting in the In Vivo Interferon Response to Listeria monocytogenes and Cyclic Dinucleotides. Infection and Immunity. 2011b; 79:688–694. [PubMed: 21098106]

Seth RB, Sun LJ, Ea CK, Chen ZJJ. Identification and characterization of MAVS, a mitochondrial antiviral signaling protein that activates NF-kappa B and IRF3. Cell. 2005; 122:669–682. [PubMed: 16125763]

Smith JS, Xu ZL, Tian J, Stevenson SC, Byrnes AP. Interaction of systemically delivered adenovirus vectors with Kupffer cells in mouse liver. Human Gene Therapy. 2008; 19:547–554. [PubMed: 18447633]

Takaoka A, Wang Z, Choi MK, Yanai H, Negishi H, Ban T, Lu Y, Miyagishi M, Kodama T, Honda K, et al. DAI (DLM-1/ZBP1) is a cytosolic DNA sensor and an activator of innate immune response. Nature. 2007; 448:501–U514. [PubMed: 17618271]

Takeuchi O, Akira S. Innate immunity to virus infection. Immunological Reviews. 2009; 227:75–86. [PubMed: 19120477]

Ting JPY, Willingham SB, Bergstralh DT. NLRs at the intersection of cell death and immunity. Nature Reviews Immunology. 2008; 8:372–379.

Upton JW, Kaiser WJ, Mocarski ES. Virus Inhibition of RIP3-Dependent Necrosis. Cell Host & Microbe. 2010; 7:302–313. [PubMed: 20413098]

Upton JW, Kaiser WJ, Mocarski ES. DAI/ZBP1/DLM-1 Complexes with RIP3 to Mediate Virus-Induced Programmed Necrosis that Is Targeted by Murine Cytomegalovirus vIRA. Cell Host & Microbe. 2012; 11:290–297. [PubMed: 22423968]

Xu LG, Wang YY, Han KJ, Li LY, Zhai ZH, Shu HB. VISA is an adapter protein required for virus-triggered IFN-beta signaling. Molecular Cell. 2005; 19:727–740. [PubMed: 16153868]

Yoneyama M, Suhara W, Fujita T. Control of IRF-3 activation by phosphorylation. Journal of Interferon and Cytokine Research. 2002; 22:73–76. [PubMed: 11846977]

Highlights

- IRF3 is a critical and non-redundant factor that executes necrotic death *in vivo*.
- IRF3 executes necrosis independently of its transcription activator function.
- IRF3-dependent necrotic cell death is distinct from pyroptosis and necroptosis.
- IRF3-dependent necrosis protects the host from disseminated virus infection.

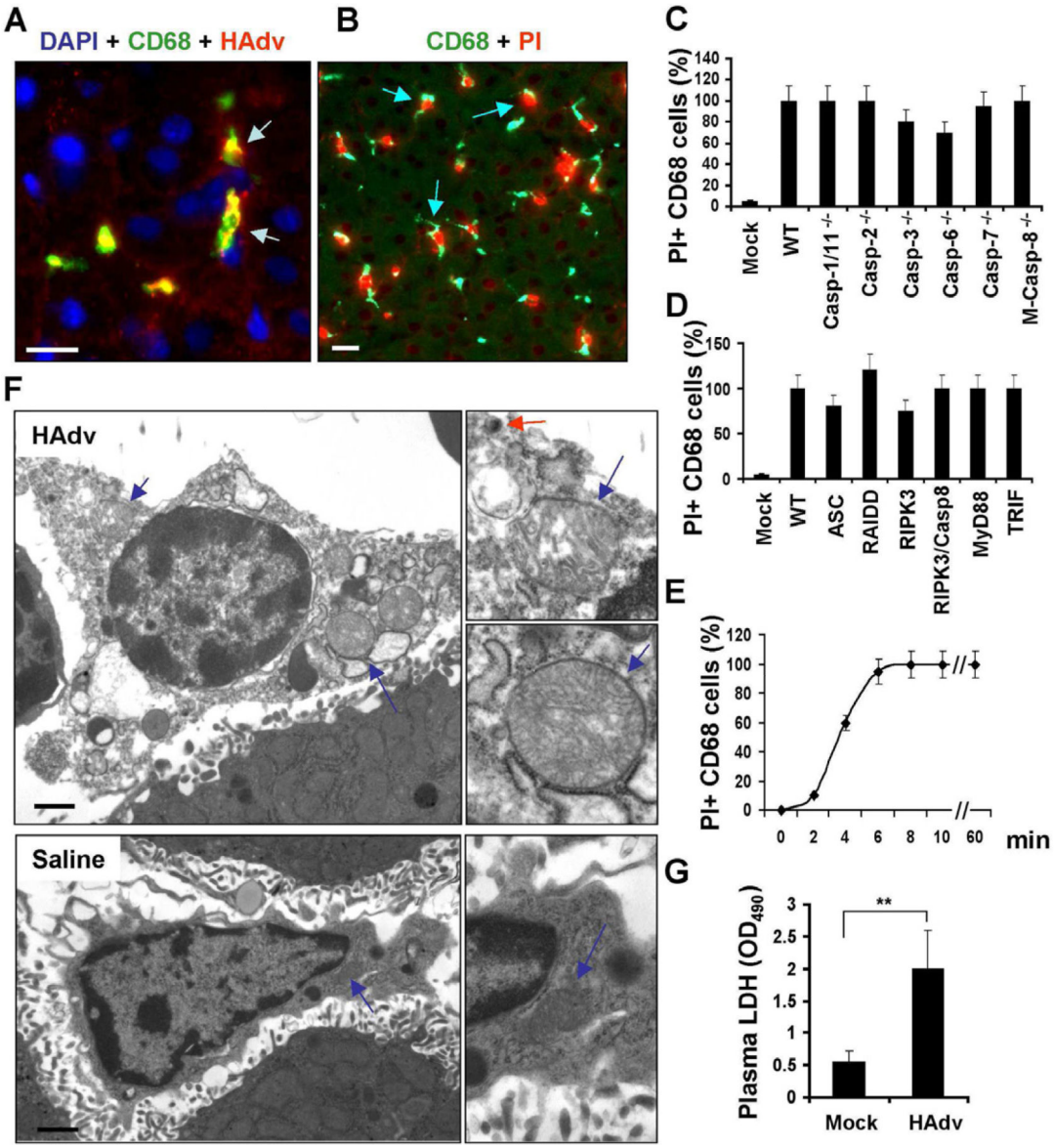

Figure 1. HAdv triggers necrotic type of macrophage death *in vivo*, independently of caspase-1, caspase-8, and RIPK3

(A) Confocal microscopy analysis of HAdv particle distribution in liver parenchyma revealed accumulation of the virus (red, indicated by arrows) in $CD68^+$ resident macrophages (green). Cell nuclei were strained with DAPI (blue). $N = 8$. The scale bar is 10 μm. **(B)** $CD68^+$ liver macrophages (green) become propidium iodide-permeable (red, indicated by arrows) after interaction with HAdv. $N = 8$. The scale bar is 10 μm. **(C-D)** The percentage of PI-permeable $CD68^+$ cells in the liver parenchyma of indicated gene-deficient mice 60 min after challenge with HAdv. Error bars represent standard deviation of the mean. *M-Casp-8*$^{-/-}$ - mice with macrophage-specific ablation of Caspase-8. $N = 8$. **(E)** Kinetics of plasma membrane integrity loss by $CD68^+$ macrophages in the livers of wild type mice after challenge with HAdv. $N = 5$. **(F)** Electron microscopy analysis of ultrastructural changes in liver macrophages 15 minutes after challenge with HAdv *in vivo*. Right panels in show the high-power images of mitochondria (blue arrows) and the virus (red arrow). The scale bar is

2 μm. $N = 5$. **(G)** Plasma LDH levels in mice mock-infected with saline or infected with HAdv 30 min post infection. $N = 5$, ** $P < 0.01$.

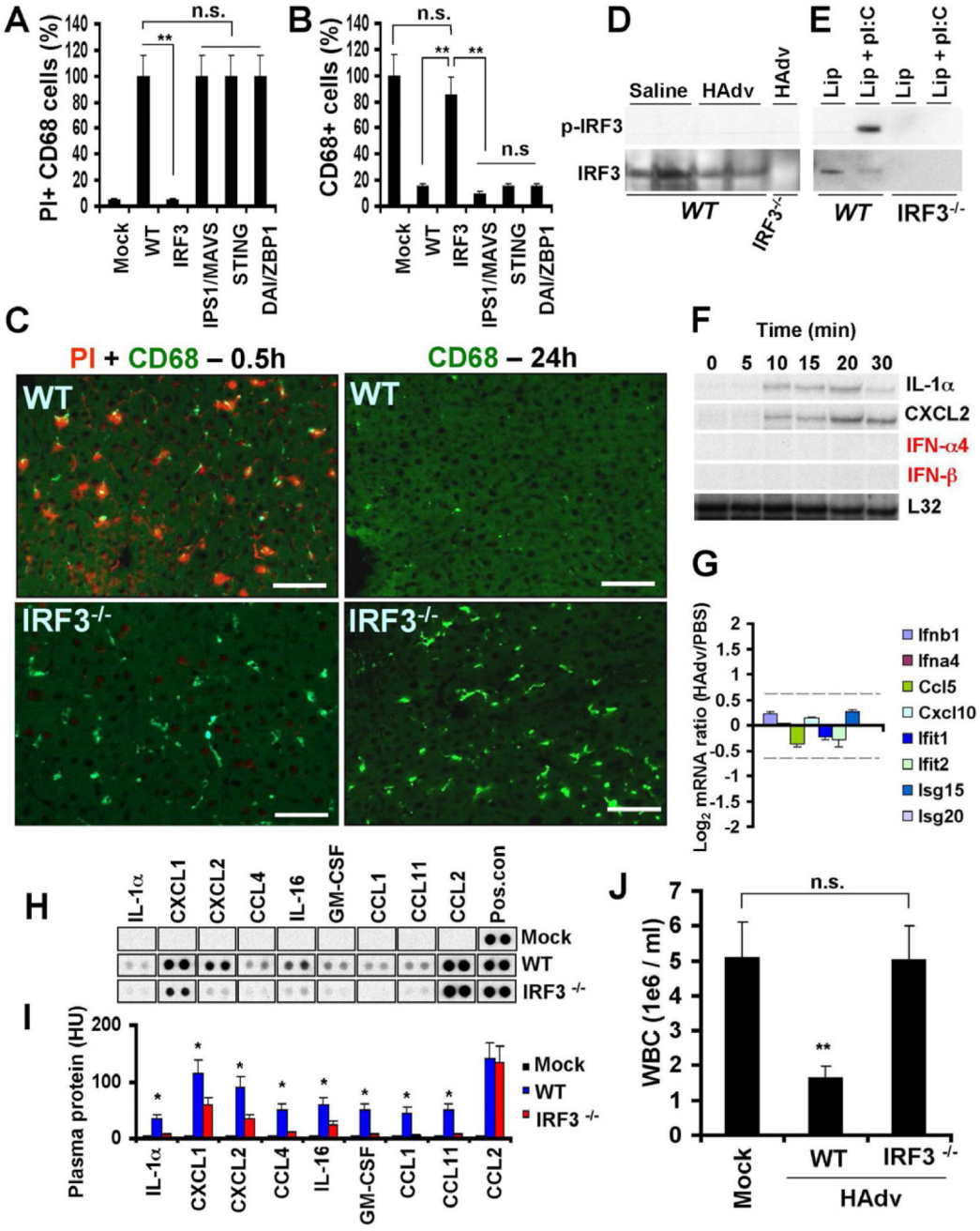

Figure 2. Macrophages in *Irf3*$^{-/-}$, but not in IPS1/MAVS- or STING-deficient mice, are resistant to virus-induced necrotic cell death

The percentage of PI-permeable CD68^{+} cells in the liver parenchyma of indicated gene-deficient mice 1 h **(A)** or 24 h **(B)** after challenge with HAdv. $N = 8$. Error bars represent standard deviation of the mean. ** - $P < 0.001$. n.s. – not statistically significant. **(C)** The sections of livers from wild type (*WT*) or *Irf3*$^{-/-}$ mice 0.5 h and 24 h after challenge with HAdv and PI were stained with anti-CD68-MAb (green) and PI (red) analyzed by fluorescent microscopy. The scale bar is 30 μm. $N = 6$. Western blot analysis of IRF3 phosphorylation at Ser 396 in the livers of mice 20 min after saline or HAdv injection **(D)** or in the mouse bone marrow-derived macrophages **(E)** from *WT* and *Irf3*$^{-/-}$ mice treated with either Lipofectamine alone (Lip) or with a mixture of Lipofectamine and poly-I:C. **(F)**

Kinetics of transcriptional activation of NF-kB-dependent IL-1α, CXCL2, and IRF3-dependent IFN-α4 and IFN-β genes in the liver of mice from 0 to 30 minutes after intravenous infection with adenovirus, determined by the RNAse protection assay. $N = 3$. **(G)** The ratio of the amounts of mRNAs for IRF3-dependent genes in the spleen of *WT* mice 30 minutes after infection with HAdv *vs.* mice injected with PBS, determined by mRNA arrays. The data for the indicated gene set was extracted from the micro-array data set collected earlier and deposited to the Gene Expression Omnibus database under the accession no. GSE36078. $N = 3$. The 1.5-fold differential expression interval is depicted with dotted lines. **(H)** The pro-inflammatory cytokines and chemokines in plasma of *WT* and *Irf3*$^{-/-}$ mice 1 hour after challenge with HAdv, determined by Proteome Profiler antibody array. $N = 4$. Mock – mice were injected with saline. Pos. con. – are dots showing manufacturer's internal positive control samples on each membrane. **(I)** Quantitative representation of the dot blot data shown in (H) analyzed by densitometry and histogram processing tool. HU – histogram units. **(J)** Total white blood cell count in the blood of *WT* and *Irf3*$^{-/-}$ mice 24 hours after challenge with HAdv. Mock – mice were injected with saline. n.s. – not statistically significant. ** $P < 0.01$. $N = 8$.

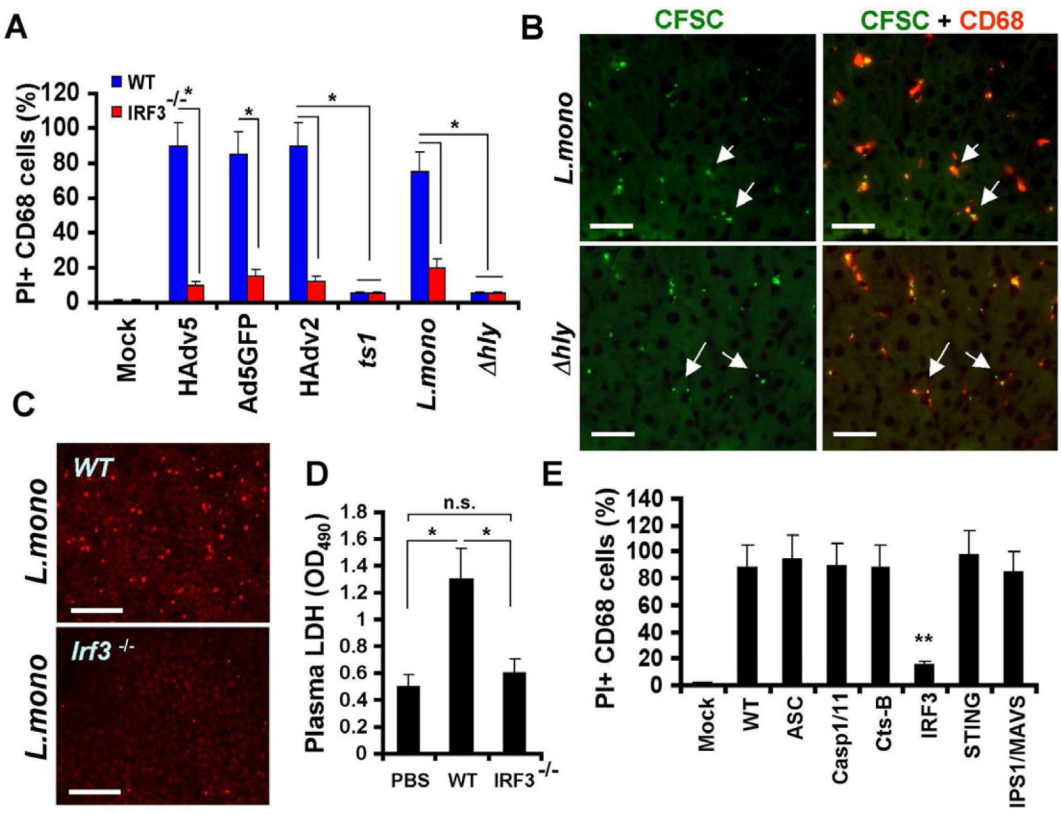

Figure 3. *L.monocytogenes* and HAdv trigger IRF3-dependent macrophage necrosis *in vivo* upon entry into the cytosol

(A) The percentage of PI-permeable CD68^{+} cells in the liver parenchyma of *WT* and *Irf3*$^{-/-}$ mice 60 minutes after challenge with indicated pathogens. $N = 6$. Error bars represent standard deviation of the mean. * - $P < 0.01$. **(B)** Immunofluorescent microscopy analysis of distribution of CFSC-labeled *L.monocytogenes* or Δ*hly* cells (green) in liver parenchyma at 30 min p.i. revealed their accumulation in CD68^{+} resident macrophages (red, indicated by arrows). $N = 8$. The scale bar is 20 μm. **(C)** Distribution of PI-permeable cells in livers of *WT* and *Irf3*$^{-/-}$ mice 1 h after *L.monocytogenes* infection. $N = 5$. Scale bar is 50 μm. **(D)** Plasma LDH levels in mice mock-infected with saline (PBS) or *WT* and *Irf3*$^{-/-}$ mice infected with *L.monocytogenes* 1 hour post infection. $N = 5$, ** $P < 0.01$. n.s. – not significant. **(E)** The percentage of PI-permeable CD68^{+} cells in the liver parenchyma of indicated gene-deficient mice 1 hour after challenge with *L.monocytogenes*. Error bars represent standard deviation of the mean. $N = 8$. Mice were injected with saline in mock-infected group (Mock). ** $P < 0.01$.

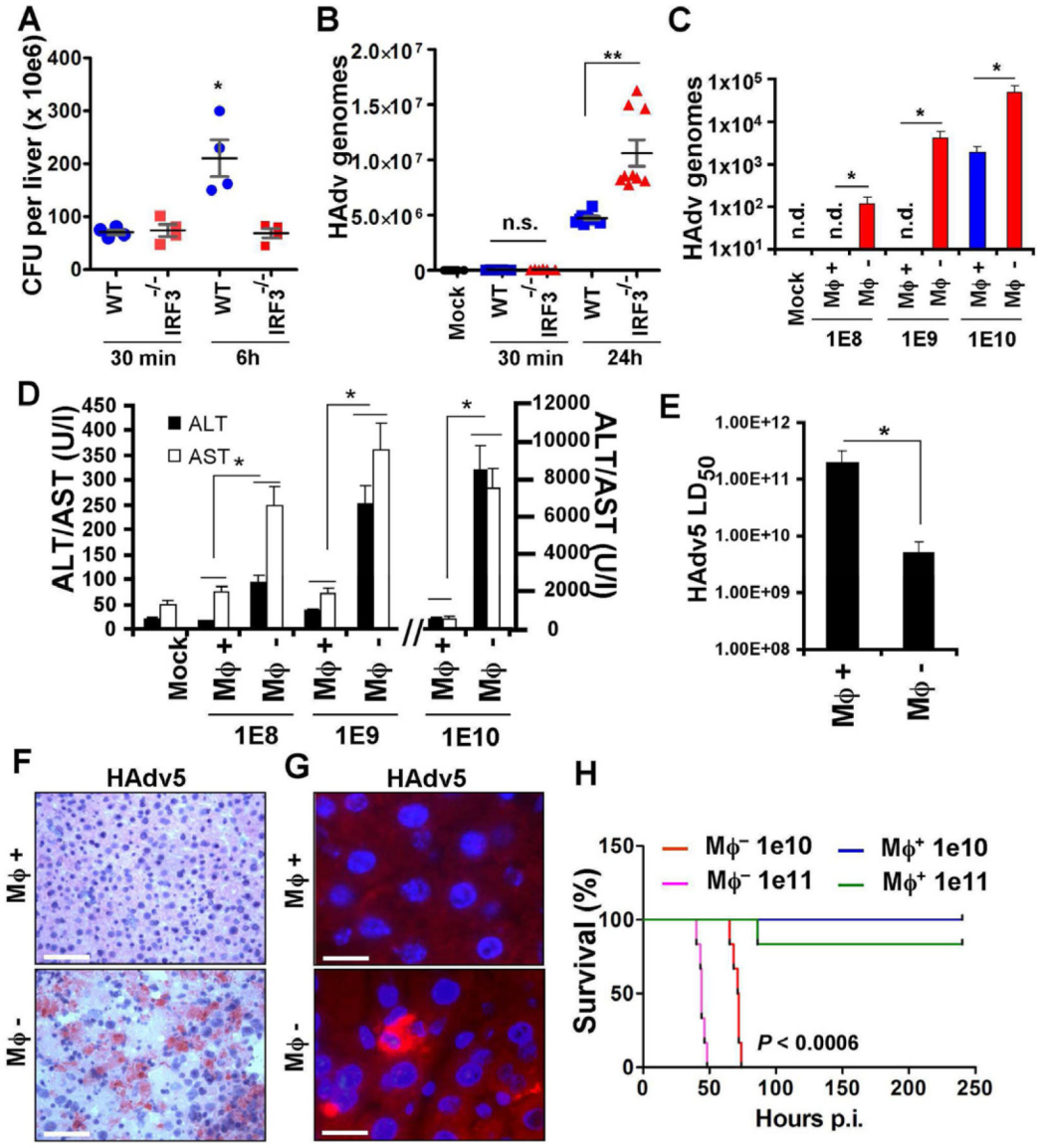

Figure 4. IRF3-dependent "defensive suicide" is a protective macrophage effector mechanism against disseminated virus infection

Pathogen burden in the livers of *WT* and *Irf3*$^{-/-}$ mice infected with *L.monocytogenes* **(A)** and wild type HAdv5 **(B)** analyzed at indicated times. Representative data from two experiments are shown. The data in (A) was analyzed by 1-way ANOVA, * $P = 0.0014$, and in (B) by 1-way ANOVA with post-hoc Kruskal-Wallis test. ** $P < 0.001$. **(C)** The amounts of the virus genomic DNA in the livers of wild type mice depleted of tissue macrophages with clodronate liposomes (Mϕ -) or mice containing tissue macrophages (Mϕ +; mice were injected with liposomes containing saline only) 48 hours after challenge with HAdv5 at indicated doses (in virus particles per mouse). The amounts of viral genomes per 10 ng of total liver DNA are shown. $N = 6$. * $P < 0.01$. **(D)** The amounts of liver enzymes ALT and AST in plasma Mϕ- and Mϕ+ mice 48 hours after challenge with HAdv5 at indicated doses. In Mock settings, ALT and AST levels were similar in Mϕ+ and Mϕ- mice prior to virus challenge. $N = 6$. * - $P < 0.01$. **(E)** Reduction of LD_{50} of HAdv5 for mice after depletion of tissue macrophages with clodronate liposomes (Mϕ-), compared to mice containing tissue macrophages (Mϕ+). $N = 9$. * $P < 0.05$. **(F)** Hematoxyllin and eosin staining of liver

sections from Mϕ+ and Mϕ- mice 48 hours after infection with 10^{10} virus particles of HAdv5. Scale bar is 100 μm. **(G)** Sections of liver as in (F) after staining with anti-HAdv5 hexon Ab (red). Cell nuclei were couterstained with DAPI (blue). Scale bar is 10 μm. **(H)** Survival of Mϕ- and Mϕ+ mice after challenge with indicated doses of HAd5. $N = 8$. Statistical significance of $P < 0.0006$ is indicated for groups of Mϕ- mice when compared to Mϕ+ mice using log-rank test.